The Preparation and Electrochemical Properties of Perovskite La$_{0.6}$Sr$_{0.4}$CoO$_{3-d}$ for Catalytic Reduction of Oxygen

Lining Fang

School of Chemical Engineering, Tianjin University, Tianjin 300072, China
E-mail: lningfang008i@foxmail.com

La$_{0.6}$Sr$_{0.4}$CoO$_{3-d}$ powder in nanoscale was produced through flame spray synthesis (FSS), which was a process method of particles in large scale. Then, the catalytic performance of the powder as a bi-functional catalyst towards oxygen evolution reaction (OER) and oxygen reduction reaction (ORR) was evaluated. The effect of this processing method on the as-prepared powders was studied through nitrogen adsorption (BET), thermal gravimetric analysis (TGA) and X-ray powder diffraction (XRD). The remarkable electrocatalytic activities were observed in all the synthesized La$_{0.6}$Sr$_{0.4}$CoO$_{3-d}$ compared with Ketjen black. Combined with the structure and electrochemical properties, a systematical study on the catalytic activity of La$_{0.6}$Sr$_{0.4}$CoO$_{3-d}$ towards both OER and ORR was carried out. Besides, the battery capacity of La$_{0.6}$Sr$_{0.4}$CoO$_{3-d}$ was investigated in a lithium-air battery as an air cathodic catalyst.

1. INTRODUCTION

In theory, a lithium-air battery possesses 10 folds of energy density compared to a lithium-ion battery. Moreover, a lithium-air battery also exhibits the advantages including the inexpensive feature and low mass as the oxygen from air is employed in the air electrode as the active material. Thus, a remarkable research interest has been attracted to apply the lithium-air battery into the large energy storage devices [1-4].

However, numerous technique problems still need to be solved so that the lithium-air battery could commercially applied. [5]. Especially, the depredation performance of lithium-air battery will take place [6, 7], as lithium peroxide (Li$_2$O$_2$) generated in the process of discharge at the cathode is in

the solid phase which would immobilize the pores on the surface of the porous carbon electrode and further decrease the contact area between the electrolyte and oxygen. Besides, Li_2O_2 serves as an insulator, resulting in the difficulty to transfer electron. Thus, to decompose Li_2O_2 and Li_2O into Li and O_2 during the recharging process needs high overpotential. However, this overpotential will induce some secondary reactions, which accelerate the decomposition of electrolyte and the corrosion of the carbon electrode. Moreover, irreversible discharging products including Li2CO3 and LiRCO3 have been demonstrated that they could result in the deterioration of the cycle life of the lithium-air battery [8-16].

So far, wide and intensive attentions have been attracted to solve these problems as well as to design novel potential catalysts with high activity at the air electrode [17, 18]. Thus, numerous metals and oxides such as Pt have been applied in the metal-air batteries and fuel cells served as air cathode catalysts [19-21]. Particularly, the perovskite oxides have also been studied recently at the air cathodes in the lithium-air batteries as a kind of active catalyst. The catalytic capacities of the perovskite oxides, such as $CaMnO_3$ [22], $La_{0.8}Sr_{0.2}BO_3$ [23], La_2NiO_4 [24], $La_{0.6}Ca_{0.4}Co_{0.8}Fe_{0.2}O_3$, $La_{0.6}Sr_{0.4}Co_{0.2}Fe_{0.8}O_3$, $La_{0.8}Sr_{0.2}Fe_{0.8}Mn_{0.2}O_3$ [25], $Ba_{0.9}Co_{0.5}Fe_{0.4}-Nb_{0.1}O_3$ [26], $LaFeO_3$ [27] and $LaNi_{1-x}Mg_xO_3$ [28] as well as the oxides which are substituted at their A and B sites, have been investigated. However, the studies have extensively done on the charge/discharge and cyclic capacities of the lithium-air batteries, where a systematic research in detail on the properties of the materials in field of electrochemistry has not been thoroughly completed. Moreover, $La_{0.6}Sr_{0.4}CoO_{3-d}$, which has primarily studied on the electrochemical features for the application in the solid fuel cells as cathode electrode to decrease the resistance of the electrode, is regarded as potential material in fuel cells [29] among all the reported perovskite catalysts, owing to the higher electronic conductivity and oxide ion conductivity in comparison with the other perovskite oxides [30]. Zhang et al. [31] reported the hierarchical mesoporous perovskite $La_{0.5}Sr_{0.5}CoO_{2.91}$ nanostructures which was applied in the Li-air batteries. They found that the $La_{0.5}Sr_{0.5}CoO_{2.91}$ composite exhibited remarkable electrochemical properties and cell capacity with an ultrahigh discharge capacity of more than 11000 mA h/g.

This work reported the synthesis of nanoscale $La_{0.6}Sr_{0.4}CoO_{3-d}$ through FSS method. With the Pechini approach, $La_{0.6}Sr_{0.4}CoO_{3-d}$ exhibited relatively high ionic and electronic conductivites. Herein, we aimed to produce and optimize the nanocrystalline powders exhibiting high specific surface area (SSA). The CV, ORR and OER measurements were performed with the as-obtained $La_{0.6}Sr_{0.4}CoO_{3-d}$ oxides, where Ketjen black and Pt/C were used as the comparative references. The charge/discharge cyclic performance of $La_{0.6}Sr_{0.4}CoO_{3-d}$ was investigated, where $La_{0.6}Sr_{0.4}CoO_{3-d}$ was applied in the air cathode of the lithium-air battery as electrocatalyst. According to the experimental analysis, the catalytic activities of the as-synthesized $La_{0.6}Sr_{0.4}CoO_{3-d}$ were investigated in the regard of their structural properties for OER and ORR.

2. EXPERIMENTAL

2.1. Flame Spray Instrument

A specific FSS approach was employed to produce the $La_{0.6}Sr_{0.4}CoO_{3-d}$ powders [32]. In general, the mixture of liquid precursor was atomized into the aerosol of fine droplet through an

adjustable oxygen flow (0.3-1.0/s, 99.95%) and then was sprayed axially with the premixed flame of acetylene and oxygen (0.2171/s C_2H_2, 99.6% and 0.2831/s O_2, 99.5%). Then, through taking samples of aerosol with a bypass on the glass fiber filters, the typical samples were gathered up to 2 g. However, the prime aerosol was collected by a pulse-jet baghouse of semi-industrial, of which the effective filtration area is 3.5 m^2.

2.2. Precursor System

The stoichiometric amounts of strontium (II) nitrate, cobalt (III) nitrate hexahydrate and lanthanum (III) nitrate hexahydrate were dissolved in a defined solvent to prepare the precursor solutions. The mixture of acetic acid and the deionized water was employed in various water-fuel ratios as solvent. Due to the innocuousness, low cost and comparably high solubility of nitrates in such mixture, acetic acid was selected in this work. As the corresponding nitrates, the cation of La:Sr:Co in stoichiometric amounts with a ratio of 6:4:10 were sequentially added into the solvent mixture which was stirred. To synthesize $La_{0.6}Sr_{0.4}CoO_{3-d}$, the concentration of precursor solution (0.75 M) was adjust

2.3. Characterizations

X-ray diffraction (PANalytical X'Pert Pro MPD, Netherlands) with Cu Ka radiation (l=1.540598 Å) was employed to characterize the crystal structure and the formation of the secondary phase. The measurements were performed in a 2q range of 20 to 80°, where the step size was 0.0167. Besides, Scherrer equation described below was employed to determine the crystallite size [33, 34].

$$d_{XRD} = \frac{K\lambda}{\beta \cos\theta}$$

In Scherrer equation, the constant shape factor was represented by K, where b meant the full width at half maximum value (FWHM) of the relevant Bragg angle.

The measurements of the cathode-electrolyte reaction were performed on the pellets, which was consisted of the mixture of $La_{0.6}Sr_{0.4}CoO_{3-d}$ and the relevant electrolyte powder in a weight ratio of 1:1. The 15 nm pellets were pressed unidirectionally to generate the close contact under the pressure of 29 MPa, which were further fired either at 800 °C for 125 h or at 1000 °C for 4 h. Then, the quantitative phase analyses were carried out through Rietveld analysis which was performed with X'pert Highscore.

As a reference, the usual $La_{0.6}Sr_{0.4}CoO_{3-d}$ materials were produced through the spray pyrolysis (SP) of the corresponding nitrates and then annealed at 1050 °C for 24 h to obtain the phase pure $La_{0.6}Sr_{0.4}CoO_{3-d}$. The powder exhibiting a particular surface area of 9 m^2/g was produced with liquid-based planetary ball milling and subsequent high energy.

Brunauer-Emmett-Teller theory (BET) was used to determine the SSA at 77K through a five-point nitrogen adsorption isotherm. Firstly, all the powders were dried with a nitrogen flow at 180 °C for 3 h. Then, SA 3100 (Coulter Electronics) was employed to analyze the powders. The diameter of

the particles which were BET-equivalent could be calculated through estimating the spherical, non-aggregated and monodispersed particles.

A computerized potentiostat instrument (model CHI660) with a three-electrode system was employed to perform the electrocatalytic measurements of OER and ORR at room temperature, where KOH solution with a concentration of 0.1 M was used as electrolyte. In the case of the cyclic voltammetry measurements, the electrode made of glassy carbon disk was used as the working electrode. However, for the linear sweep voltammetry (LSV), the measurements were performed at a scanning rate of 5 mV/s and a disk rotating rate of 1600 rpm, where a rotating ring glassy carbon disk electrode (RRDE) with a diameter of 5.61 mm was employed as the working electrode.

2.4. Electrode preparation

The as-prepared $La_{0.6}Sr_{0.4}CoO_{3-d}$ in this work was employed as the catalyst for the air cathode, where KB (Ketjen Black, EC600JD) and Pt/C (30 wt%, Premetek Co.) were used as references. To study the CV, OER and ORR, the as-produced $La_{0.6}Sr_{0.4}CoO_{3-d}$ and the carbon powder were mixed together in a mass ratio of 3 to 7 so that to obtain adequate electronic conductivity. In general, the as-prepared catalyst (10 mg) was dispersed into the diluted nafion solution in isopropyl alcohol (150 mL) with a concentration of 5 wt%. Then a part of the suspension (13.5 mL) was deposited onto a glassy carbon substrate with pipette. Moreover, the Pt wire was employed as the counter electrode, where Hg/HgO acted as the reference electrode. Noted that oxygen needed to be bubbled into the cell directly for more than one hour before the measurements.

To study the lithium-air battery, the as-prepared $La_{0.6}Sr_{0.4}CoO_{3-d}$ catalyst and KB were mixed together in a ratio of 1:2 to prepare the air cathodes with the teflonized acetylene black (binder) in isopropyl alcohol. The mixture was produced to generate a fine pellet with a diameter of around 1 cm. Then the pellet was further pressed on a current collector made of Ni mesh, of which the diameter was 1.2 cm. Subsequently, the as-produced electrode was dried at 100 ^{o}C for 12 hours under vacuum, which was further employed as the air cathode in a Li-air battery. The lithium foil was employed as an anode, where LiTFSI with a concentration of 1 M was dissolved in TEGDME to prepare the electrolyte. To fabricate the lithium-air battery, a Swagelok test cell was employed. Then, the cell test was performed under an oxygen flow of 10 cm^3/min, where the current density is 0.1 mA/cm^2 with a cut-off voltage ranging from 2.0 to 4.3 V.

3. RESULT AND DISCUSSION

The synthesis conditions not only affected the powder quality such as the phase purity and uniformity, but also significantly influenced the size distribution of particles and the SSA. Here, we intended to produce nanoscale powder in cost-efficient large-scale production. The specific surface area of the later cathode powders was restricted to below 40 m^2/g as they were processed as the screen

printing pastes. Because of the solid loading and viscosity of the resultant paste, the stabilization was critical for the powders with relatively higher SSA, which could be counterproductive.

Figure 1 illustrated the relationship between the production of the powders by FSS and the ratio of acetic acid to water. As shown in Figure 1, the nitrates in pure water primarily generated the expected $La_{0.6}Sr_{0.4}CoO_{3-d}$ phase (PDF code 01-089-5719) [35]. Nevertheless, the secondary phase, which was recognized as $(La, Sr)2CoO4$ (PDF code 01-83-2411) [36], was observed in the system. The content of $(La, Sr)2CoO4$ was determined to be 31 wt% according to the quantitative phase analysis and the deconvolution of XRD spectra. The combustible parts of the solvent mixture remarkably determined the amount of the secondary phase (Figure 2). The flame was cooled down by the pure water, which would restrict the homogeneous mixing among the elements in the particles at the atomic level. Moreover, in the solvent, each single nitrate exhibited a diverse solubility, resulting in the precipitation on the surface of the sprayed droplet during the process of evaporation [37].

When the fraction of acetic acid increased up to 70 vol.% from 0, the powders produced by the flame synthesis became gradually better particles possessing higher SSA, accompanied with a least generation of $(La, Sr)_2CoO_4$. Besides, more combustion enthalpy was supplied to the flame reactor when the fraction of acetic acid increased, resulting in the dilution of the aerosol by gaseous H_2O and CO_2 which were generated from the decomposition of acetic acid. A linear increase of SSA from 17 m^2/g (60 nm) to 39 m^2/g (24 nm) was induced by these effects which also resulted in that the morphology of particles became more homogeneous. Besides, the spherical and crystalline particles in nanoscale became predominant, whereas the particles with large irregular shape and several microns decreased. However, the bimodal particle size distribution was still observed, where around 10 vol% of the powder were composed of massive spherical particles with a size of 50-200 nm.

Moreover, the formation of the secondary phase was also influenced by the increased energy which transferred from combustible acetic acid with higher fractions into the flame. As shown in Figure 2, the optimized condition was found to be 30 vol.% acetic acid aqueous solution, resulting in that the content of $(La,Sr)_2CoO_4$ decreased to 12 wt% from the original 27 wt%. However, it was observed that $(La,Sr)2CoO4$ increased moderately again, which might be caused by the enhanced evaporation of cobalt. Besides, it also might be induced by the flame conditions which became gradually harsher, including that the temperatures of flame became higher and the retention times in the flame became longer because the combustible substances with larger amount enlarged the flame height. Nevertheless, during the process of the flame synthesis, or more specifically in the period of the cooling phase, cobalt would again precipitate on the generated nanoparticles through the so-called polyphase condensation process. Such cobalt evaporation was general and widespread in the powder processing, where the precise control of the synthesis conditions was required. Moreover, several nanopowders such as $La_{0.6}Sr_{0.4}Co_{0.2}Fe_{0.8}O_3$ and $Ba_{0.5}Sr_{0.5}Co_{0.8}Fe_{0.2}O_3$ were demonstrated in our previous study through element analysis with inductively coupled plasma optical emission spectroscopy (ICP-OES) that the presumed and expected cobalt took place and would not disappear. Overall, these results indicated that the cobalt might be in the amorphous state.
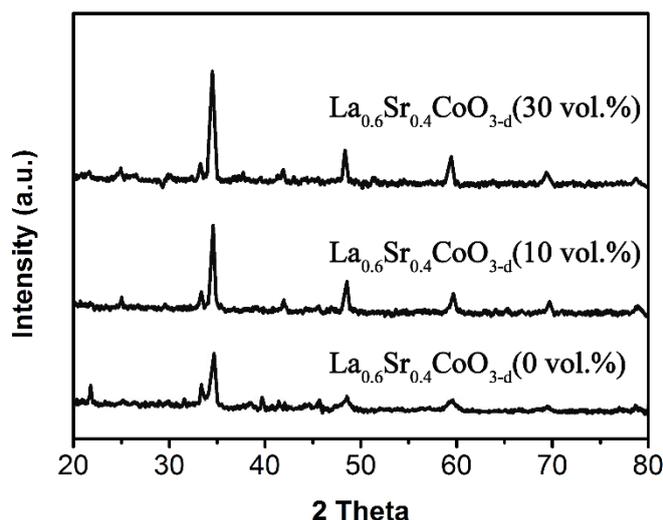
Figure 1. Diffraction patterns of the as-synthesized $La_{0.6}Sr_{0.4}CoO_{3-d}$ powders towards the volume fraction of the combustible acetic acid (0-70 vol.%). $La_{0.6}Sr_{0.4}CoO_3$ and $(La,Sr)_2CoO_4$ are indicated by the peak position and intensity at the bottom as references.
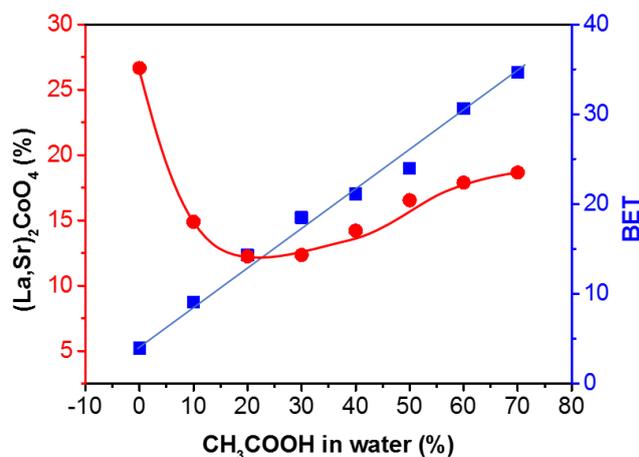

Figure 2. The relationship among the amount of the secondary $(La,Sr)_2CoO_4$ phase in the obtained $La_{0.6}Sr_{0.4}CoO_{3-d}$ powders and the fraction of combustible acetic acid and the relevant BET.

TGA was employed to analyze the as-prepared nanopowders. As shown in Figure3, it was demonstrated that the combustible solvent with a definite fraction was required to ensure the improved decomposition of the precursor. A total mass loss was measured to be 13.7 wt% beginning with the nitrates dissolved in the pure water. The mass loss could be reduced remarkably when the fraction of acetic acid increased. The mass loss, which was induced by the undecomposed residues, decreased to 9.63 and 4.6 wt% when the fractions of acetic acid in the solvent mixture were 10 and 30 vol.%, respectively. However, no further reduction would be caused by the acetic acid with higher fraction. All the as-synthesized powders by physisorbed water exhibited an original mass loss under the

synthesis condition at the temperature in the range of room temperature to 180 ^{o}C. Subsequently with the gradually increased temperature up to 750 ^{o}C, the mass loss related to the solvent fraction presented, which originated from some overlapped decomposition procedures of the intermediates. Especially, a slight mass loss around 0.1 wt% was further observed, which was induced by the change of the non-stoichiometry oxygen in $La_{0.6}Sr_{0.4}CoO_{3-d}$ driven by the temperature. This was typical for such perovskite materials through compensating the changes of valence state. Because of the super-position with the precursor-caused mass loss, the d changed remarkably when the temperature was high, although it would change with the variation of temperature in the whole range. However, the core-shell, hollow and porous particles increased when acetic acid decreased, which were produced through the precipitation of nitrates [38]. The resultant large mass loss could be ascribed to that the precursors in such hollow or porous particles were partially enclosed and survived during the process of flame spray. Such a different behavior is related to the change in the nature of the adsorbed oxygen species on the transition metal cations and to the type of interactions for molecular oxygen on the electrocatalyst surface of different perovskites [39]. Moreover, the combustion of acetic acid disrupted the droplets more efficiently when the amounts of acetic acid increased, where the transfer from liquid to gas got less restricted, resulting in the generation of more homogenous powder in nanoscale.
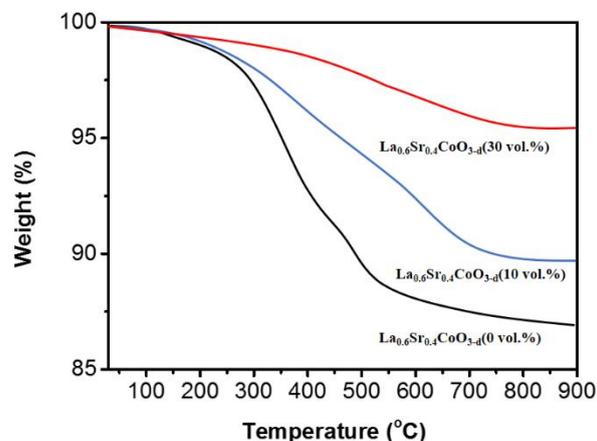

Figure 3. TGA analyses of the as-synthesized $La_{0.6}Sr_{0.4}CoO_{3-d}$ powders with acetic acid aqueous solution in various fraction (0, 10 and 30 vol.%).

The electrocatalytic capacity of the perovskite $La_{0.6}Sr_{0.4}CoO_{3-d}$ produced with a varied fraction of acetic acid in water (0, 10 and 30 vol.%). The cyclic voltammogram of the perovskite $La_{0.6}Sr_{0.4}CoO_{3-d}$ was illustrated in Figure 4, which was measured in oxygen-saturated KOH solution with a concentration of 0.1 M, where the scanning rate was 50 mV/s. In the case of both the 10 vol.% and 30 vol.% samples, a peak almost at the same potential in the cathodic reduction curves was observed. Furthermore, the CV curve of 30 vol.% sample, which was measured under N_2 atmosphere, exhibited the characteristic of the two-layer capacitance in absence of the peak evolution. It indicated that the peak recorded at O_2 atmosphere was induced by the ORR at the cathode. Based on the CV curves shown in Table 1 and Figure 4, the current and peak potential were calculated, where no

obvious difference was observed among the peak potentials of the $La_{0.6}Sr_{0.4}CoO_{3-d}$ prepared with diverse conditions.

Table 1. Specific surface area of $La_{0.6}Sr_{0.4}CoO_{3-d}$; Peak potential, peak current, CVs onset potential and limiting current in the ORR curves of $La_{0.6}Sr_{0.4}CoO_{3-d}$ perovskite catalysts.

Sample	Specific surface area (m^2/g)	Peak potential (V)	Peak current (mA)	Onset potential (V)	Limiting current (mA)
0 vol.%	2.11	-0.21	0.112	-0.154	0.935
10 vol.%	2.57	-0.21	0.177	-0.147	0.922
30 vol.%	3.56	-0.21	0.241	-0.145	0.905

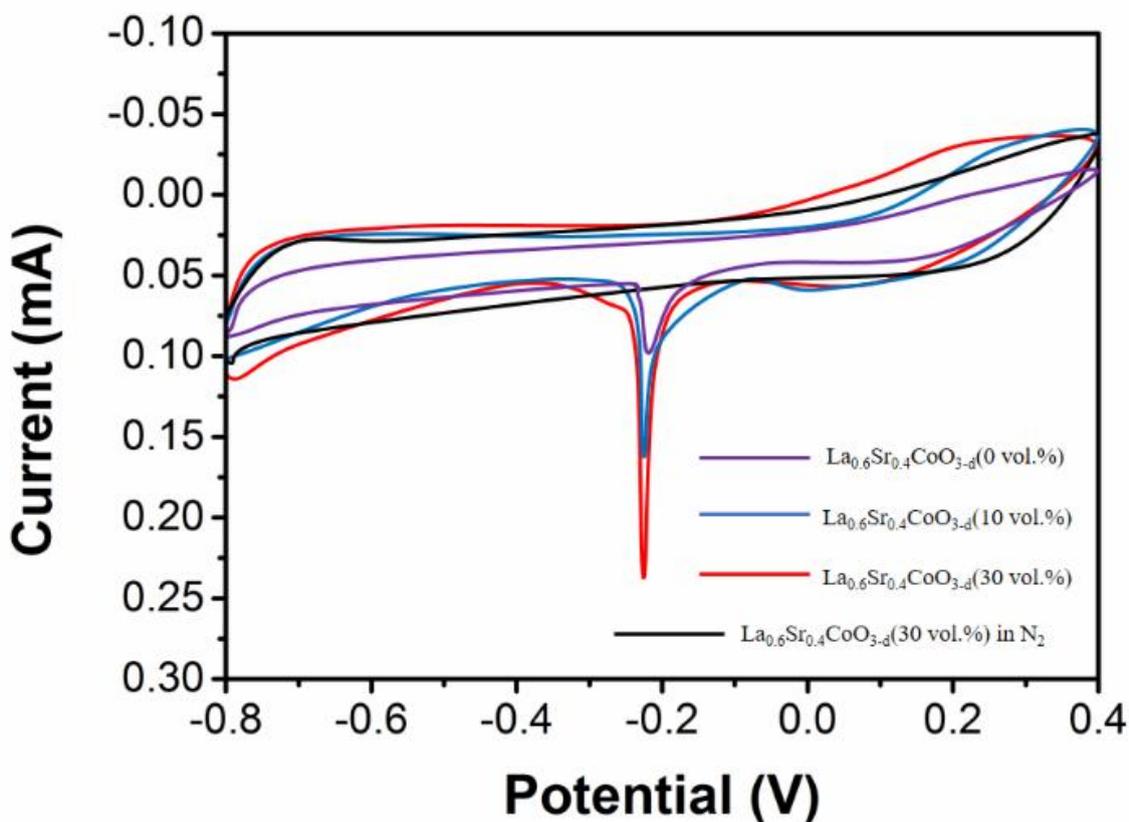**Figure 4.** Cyclic voltammogram of the perovskite catalyst $La_{0.6}Sr_{0.4}CoO_{3-d}$ in O_2-saturated KOH solution with a concentration of 0.1 M at 50 mV/s.

As shown in the left side of Figure 5, the measurements of the linear sweeping voltammogram were also employed to study the catalytic activity of the as-prepared $La_{0.6}Sr_{0.4}CoO_{3-d}$ for ORR, which were carried out in oxygen-saturated KOH solution with a concentration of 0.1 M, where the scaning rate is 5 mV/s with an electrode rotation rate of 1600 rpm. Here, the ORR activities of KB and Pt/C were also measured under the same experimental conditions as references. The onset potential and

limiting current of $La_{0.6}Sr_{0.4}CoO_{3-d}$ were superior to that of KB but inferior to that of Pt/C. Based on the data of onset potential, a lower potential was observed in $La_{0.6}Sr_{0.4}CoO_{3-d}$ (0 vol.%) for ORR compared with $La_{0.6}Sr_{0.4}CoO_{3-d}$ (10 vol.%). Although the SSA of $La_{0.6}Sr_{0.4}CoO_{3-d}$ (10 vol.%) was lower than that of $La_{0.6}Sr_{0.4}CoO_{3-d}$ (30 vol.%), a higher limiting current (0.986 mA) was obtained with $La_{0.6}Sr_{0.4}CoO_{3-d}$ (10 vol.%) compared to $La_{0.6}Sr_{0.4}CoO_{3-d}$ with a fraction of 30% (0.817 mA). However, these obtained results were induced again by the $SrCO3$ impurity which presented in $La_{0.6}Sr_{0.4}CoO_{3-d}$ (10 vol.%). Hence, the impurities were considered as the main influence on the catalytic activity instead of the SSA. For the catalytic reactions, the SSA and the chemical properties of the used catalysts were essential factors to determine the catalytic activity [40]. Generally, the catalytic capacity increased when increasing the SSA, although the amount of the active sites on the surface of catalysts was more crucial to determine the catalytic performance. Hence, more fundamental research like the study on the surface state of $La_{0.6}Sr_{0.4}CoO_{3-d}$ were required to classify this process clearly.

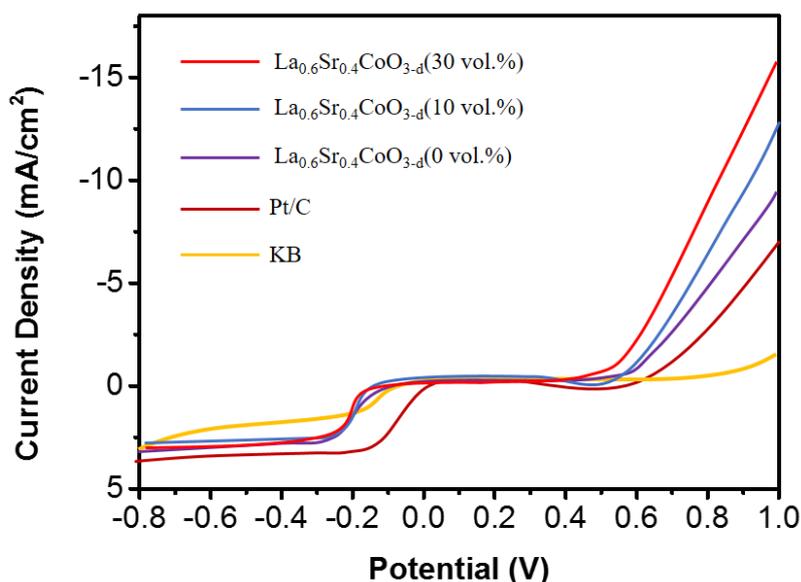**Figure 5.** The activities of oxygen electrode with the potential windows of ORR reduction and OER catalyzed by the perovskite $La_{0.6}Sr_{0.4}CoO_3$ in the oxygen-saturated KOH solution with a concentration of 0.1 M at 1600 rpm with a scan rate of 5 mV/s.

Furthermore, the catalytic performances for OER of the as-prepared perovskite catalysts were also studied. The right side of Figure 5 illustrated the polarization curves, which were collected in the period of the scanning anodic potential increased up to 1.0 V in comparison with Hg/HgO in KOH solution with a concentration of 0.1 M where the scanning and rotation rates were 5 mV/s and 1600 rpm respectively. According to the OER characteristics, a significantly better catalytic activity for OER was observed with all the as-prepared perovskite catalysts in comparison with Pt/C and KB. The total electrochemical reaction in the lithium-air battery could be classified by the equation $2(Li^+ + e^-) + O_2 = Li_2O_2$ when the oxygen ORR presented in the discharging process, whereas the Subsequent OER took place in the charging process. In general, large potential was required to decompose the solid-state discharging products-Li_2O_2 in the charging process, resulting in reducing the cycle efficiency of

the battery. Thus, the development of the effective bifunctional electrocatalyst for ORR and OER was essential for the reduction of the overpotential in the lithium-air batteries. All the as-synthesized $La_{0.6}Sr_{0.4}CoO_{3-d}$ in this work exhibited more excellent catalytic performances for ORR as well as OER compared with Pt/t and KB, which indicated that the perovskite catalysts could be used as the effective cathode catalyst in the lithium-air batteries. Moreover, considering the higher round-trip efficiency and excellent long-term stability as well as lower cost compared with noble metal catalysts, the proposed materials are a promising catalyst for the Li-air battery, especially for the oxygen evolution reaction.

The perovskite oxide catalysts were applied to the Li-air battery, as they were demonstrated with the LSV and other electrochemical characterization to possess the activities for the ORR and OER. Thus, the as-prepared perovskite catalysts were used to construct the lithium-air battery. Then, LiTFSI (TEGDME) with a concentration of 1 M in SwagelokTM type celss was employed to evaluate the charge-discharge capacity of the battery. The measurements of the cells were performed at room temperature and oxygen atmosphere in a potential range of 2.0-4.3 V, where a constant current with a density of 0.1 mA/cm^2 was utilized. Figure 6 illustrated the first charge-discharge profiles of the KB-air cathode, where the KB-air cathode was measured in the presence and absence of catalyst compared with lithium-metal anode (Li/Li$^+$). As shown in Figure 6, it was obvious that the capacity of the cells was increased with the addition of catalysts. Especially, the first discharge of $La_{0.6}Sr_{0.4}CoO_{3-d}$ (30 vol.%) reached up to a maximum capacity of about 4451 mAh/g where the voltage at discharge plateau was 2.75 V, which was remarkably higher compared with the Li-O$_2$ in the presence of $La_{0.6}Sr_{0.4}CoO_{3-d}$ with a fraction of 10 vol.% (~3057 mAh/g) and 0 vol.% (~2674 mAh/g). Besides, it was obvious that the addition of acetic acid improved the specific capacity, which also reduced the overpotential of the Li-air battery. Hence, it indicated that the capacity of the cell was improved efficiently by adding the perovskite $La_{0.6}Sr_{0.4}CoO_{3-d}$ catalyst. Table 2 shows the performance comparison of the proposed catalyst with other reports.

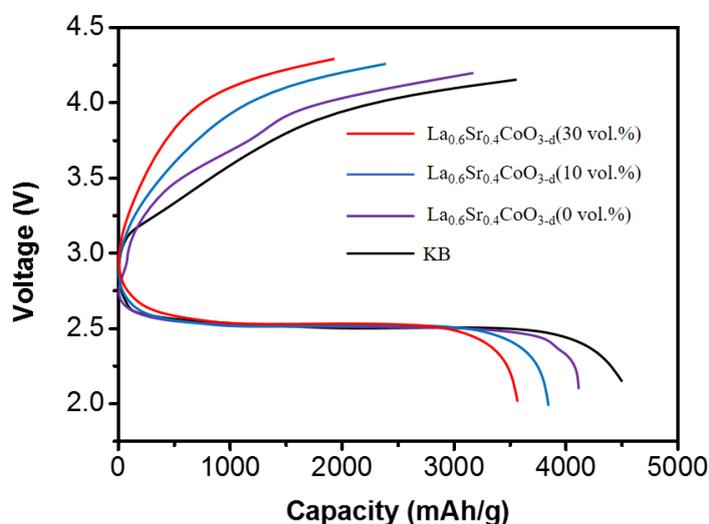**Figure 6.** Li-air battery performance of the Li–O$_2$ battery catalyzed by $La_{0.6}Sr_{0.4}CoO_{3-d}$ compared with the Li-O$_2$ battery using other catalysts.

Table 2. Specific surface area of $La_{0.6}Sr_{0.4}CoO_{3-d}$; Peak potential, peak current, CVs onset potential and limiting current in the ORR curves of $La_{0.6}Sr_{0.4}CoO_{3-d}$ perovskite catalysts.

Catalyst	Current	Discharge capacity	Reference
$La_{0.8}Sr_{0.2}MnO_3$	0.4 mA/cm^2	8890 mAh/g	[41]
$Sr_{0.95}Ce_{0.05}CoO_{3-\delta}$	0.05mA/cm^2	1500 mAh/g	[42]
$Ba_{0.9}Co_{0.5}Fe_{0.4}Nb_{0.1}O_3$	0.1 mA/cm^2	1235 mAh/g	[43]
$La_{0.6}Sr_{0.4}CoO_{3-d}$	0.1 mA/cm^2	4451 mAh/g	This work

4. CONCLUSION

The flame spray synthesis approach was employed to produce the $La_{0.6}Sr_{0.4}CoO_{3-d}$ powder in nanoscale at the level of industry relevant large-scale production. The cost-efficient nitrates, which was utilized as the precursor, was dissolved in aqueous acetic acid (30 vol.%). These conditions were considered as an optimum for inhibition of the formation of the secondary $(La, Sr)_2CoO_4$ phase, which could also improve the uniformity of the powder. According to the electrochemical characterizations, the pervosikte $La0.6Sr_{0.4}CoO_{3-d}$ displayed a remarkable catalytic capacity compared to the conventional KB. Particularly, a better catalytic activity was obtained with $La_{0.6}Sr_{0.4}CoO_{3-d}$ (30 vol.%) compared with $La_{0.6}Sr_{0.4}CoO_{3-d}$ (10 vol.%). These promising results indicated that the as-prepared perovskite $La_{0.6}Sr_{0.4}CoO_{3-d}$ could be applied to the next generation of lithium-air batteries as an air cathode.

Reference

1. E. Hosono, T. Kudo, I. Honma, H. Matsuda and H. Zhou, *Nano letters*, 9 (2009) 1045
2. J. Xiao, D. Wang, W. Xu, D. Wang, R.E. Williford, J. Liu and J.-G. Zhang, *Journal of The Electrochemical Society*, 157 (2010) A487
3. H.R. Bak, J.H. Lee, B.K. Kim and W.Y. Yoon, *Electron. Mater. Lett.*, 9 (2013) 195
4. M. Dresselhaus and I. Thomas, *Nature*, 414 (2001) 332
5. J. Coey, M. Viret and S. Von Molnar, *Advances in physics*, 58 (2009) 571
6. G. Girishkumar, B. McCloskey, A. Luntz, S. Swanson and W. Wilcke, *The Journal of Physical Chemistry Letters*, 1 (2010) 2193
7. C. Park, S. Park, S. Lee, H. Lee, H. Jang and W. Cho, *B Kor Chem Soc*, 31 (2010) 3221
8. H.-G. Jung, J. Hassoun, J.-B. Park, Y.-K. Sun and B. Scrosati, *Nature chemistry*, 4 (2012) 579
9. B. McCloskey, A. Speidel, R. Scheffler, D. Miller, V. Viswanathan, J. Hummelshøj, J. Nørskov and A. Luntz, *The journal of physical chemistry letters*, 3 (2012) 997
10. Y. Shao, S. Park, J. Xiao, J.-G. Zhang, Y. Wang and J. Liu, *Acs Catalysis*, 2 (2012) 844
11. B. Kumar, J. Kumar, R. Leese, J.P. Fellner, S.J. Rodrigues and K. Abraham, *Journal of The Electrochemical Society*, 157 (2010) A50
12. N. Eliason, S. Das and S. Seal, *Journal of Nano Education*, 8 (2016) 63
13. P.K. Rastogi and V. Ganesan, *Energy and Environment Focus*, 4 (2015) 221
14. K. Sakaushi, T.P. Fellinger and M. Antonietti, *ChemSusChem*, 8 (2015) 1156
15. B. Shin, S. Choi and Y. Tak, *Int. J. Electrochem. Sci*, 11 (2016) 5900
16. S.W. Sweeney, G. Roseman, C.P. Deming, N. Wang, T.A. Nguyen, G.L. Millhauser and S. Chen, *International Journal of Hydrogen Energy*, 41 (2016) 18005
17. A. Débart, J. Bao, G. Armstrong and P.G. Bruce, *Journal of Power Sources*, 174 (2007) 1177

18. Y.-C. Lu, Z. Xu, H.A. Gasteiger, S. Chen, K. Hamad-Schifferli and Y. Shao-Horn, *Journal of the American Chemical Society*, 132 (2010) 12170
19. A. Débart, A.J. Paterson, J. Bao and P.G. Bruce, *Angewandte Chemie*, 120 (2008) 4597
20. H. Cheng and K. Scott, *Journal of Power Sources*, 195 (2010) 1370
21. V.M.B. Crisostomo, J.K. Ngala, S. Alia, A. Dobley, C. Morein, C.-H. Chen, X. Shen and S.L. Suib, *Chemistry of Materials*, 19 (2007) 1832
22. X. Han, Y. Hu, J. Yang, F. Cheng and J. Chen, *Chemical Communications*, 50 (2014) 1497
23. J.J. Xu, D. Xu, Z.L. Wang, H.G. Wang, L.L. Zhang and X.B. Zhang, *Angewandte Chemie International Edition*, 52 (2013) 3887
24. K.-N. Jung, J.-H. Jung, W.B. Im, S. Yoon, K.-H. Shin and J.-W. Lee, *ACS applied materials & interfaces*, 5 (2013) 9902
25. H. Ohkuma, I. Uechi, N. Imanishi, A. Hirano, Y. Takeda and O. Yamamoto, *Journal of Power Sources*, 223 (2013) 319
26. C. Jin, Z. Yang, X. Cao, F. Lu and R. Yang, *International Journal of Hydrogen Energy*, 39 (2014) 2526
27. J.-J. Xu, Z.-L. Wang, D. Xu, F.-Z. Meng and X.-B. Zhang, *Energy & Environmental Science*, 7 (2014) 2213
28. Z. Du, P. Yang, L. Wang, Y. Lu, J. Goodenough, J. Zhang and D. Zhang, *Journal of Power Sources*, 265 (2014) 91
29. E. Bucher, W. Sitte, F. Klauser and E. Bertel, *Solid State Ionics*, 208 (2012) 43
30. T. Nakamura, M. Misono and Y. Yoneda, *Bulletin of the Chemical Society of Japan*, 55 (1982) 394
31. Y. Zhao, L. Xu, L. Mai, C. Han, Q. An, X. Xu, X. Liu and Q. Zhang, *Proceedings of the National Academy of Sciences*, 109 (2012) 19569
32. A. Heel, P. Holtappels, P. Hug and T. Graule, *Fuel Cells*, 10 (2010) 419
33. A. Patterson, *Physical review*, 56 (1939) 978
34. P. Scherrer, Bestimmung der inneren Struktur und der Größe von Kolloidteilchen mittels Röntgenstrahlen, Kolloidchemie Ein Lehrbuch, Springer1912, pp. 387.
35. R. Sonntag, S. Neov, V. Kozhukharov, D. Neov and J. Ten Elshof, *Physica B: Condensed Matter*, 241 (1997) 393
36. G. Demazeau, P. Courbin, G. Flem, M. Pouchard, P. Hagenmuller, J. Soubeyroux, I. Main and G. Robins, *Nouveau Journal de Chimie-New Journal of Chemistry* 3 (1979) 171
37. G.L. Messing, S.C. Zhang and G.V. Jayanthi, *Journal of the American Ceramic Society*, 76 (1993) 2707
38. R. Jossen, R. Mueller, S.E. Pratsinis, M. Watson and M.K. Akhtar, *Nanotechnology*, 16 (2005) S609
39. C. Jin, X. Cao, F. Lu, Z. Yang and R. Yang, *international journal of hydrogen energy*, 38 (2013) 10389
40. W. Zhou, Z. Shao, R. Ran, H. Gu, W. Jin and N. Xu, *Journal of the American Ceramic Society*, 91 (2008) 1155
41. F. Lu, Y. Wang, C. Jin, F. Li, R. Yang and F. Chen, *Journal of Power Sources*, 293 (2015) 726
42. W. Yang, J. Salim, S. Li, C. Sun, L. Chen, J.B. Goodenough and Y. Kim, *Journal of Materials Chemistry*, 22 (2012) 18902
43. C. Jin, Z. Yang, X. Cao, F. Lu and R. Yang, *International Journal of Hydrogen Energy*, 39 (2014) 2526